Supplemental Material for "Accessing phonon polaritons in hyperbolic crystals by ARPES"

Andrea Tomadin,[1] Alessandro Principi,[2] Justin C.W. Song,[3] Leonid S. Levitov,[4,*] and Marco Polini[1,5,†]

[1] *NEST, Istituto Nanoscienze-CNR and Scuola Normale Superiore, I-56126 Pisa, Italy*
[2] *Department of Physics and Astronomy, University of Missouri, Columbia, Missouri 65211, USA*
[3] *Walter Burke Institute for Theoretical Physics and Institute for Quantum Information and Matter, California Institute of Technology, Pasadena, CA 91125, USA*
[4] *Department of Physics, Massachusetts Institute of Technology, Cambridge, Massachusetts 02139, USA*
[5] *Istituto Italiano di Tecnologia, Graphene Labs, Via Morego 30, I-16163 Genova, Italy*

In this Supplemental Material File we present i) analytical details on the Coulomb interaction potential dressed by the presence of an anisotropic dielectric, ii) numerical and analytical results on the dispersion of the phonon-polariton modes, and iii) numerical results on the quasiparticle decay rates and spectral function as the Fermi energy and the dielectric thickness are varied.

I. ELECTROSTATICS AND FREQUENCY-DEPENDENCE OF THE HBN DIELECTRIC TENSOR

We consider a vertical heterostructure [inset of Fig. 2(b) in the main text] composed of a graphene sheet located at $z = 0$ and placed over a homogeneous but *anisotropic* insulator of thickness d with dielectric tensor $\hat{\boldsymbol{\epsilon}} = \mathrm{diag}(\epsilon_x, \epsilon_y, \epsilon_z)$. Homogeneous and isotropic insulators with dielectric constants ϵ_a and ϵ_b fill the two half-spaces $z > 0$ and $z < -d$, respectively. We calculate the electrical potential created by an electron in graphene for arbitary values of $\epsilon_x \neq \epsilon_y$ and then specialize our result to the case of a uniaxial crystal with $\epsilon_x = \epsilon_y$, such as hBN.

The electrical potential can be calculated from the following elementary approach. The displacement field $\boldsymbol{D}(\boldsymbol{r}, z)$ must satisty the condition $\boldsymbol{\nabla}\cdot\boldsymbol{D}(\boldsymbol{r}, z) = 0$ everywhere in space. However, the presence of an electron with charge density $-e\delta^2(\boldsymbol{r})\delta(z)$ at $z = 0$ implies a discontinuity of the normal component D_z of the displacement field across $z = 0$, while the tangential components E_x, E_y of the electric field $\boldsymbol{E}(\boldsymbol{r}, z)$ must be continuous.

Since the electric field $\boldsymbol{E}(\boldsymbol{r}, z)$ is irrotational everywhere in space, we can introduce the electric potential $V(\boldsymbol{r}, z)$ in the three regions of space $z > 0$, $-d < z < 0$, and $z < -d$. The Laplace equation $-\epsilon_x\partial_x^2 V(\boldsymbol{r}, z) - \epsilon_y\partial_y^2 V(\boldsymbol{r}, z) - \epsilon_z\partial_z^2 V(\boldsymbol{r}, z) = 0$ in the anisotropic dielectric (i.e. for $-d < z < 0$) can be reduced [1] to an ordinary Laplace equation by scaling $x \to x/\sqrt{\epsilon_x}$, $y \to y/\sqrt{\epsilon_y}$, and $z \to z/\sqrt{\epsilon_z}$. Imposing the aforementioned boundary conditions and carrying out elementary algebraic steps, we find the 2D Fourier transform $V_{\boldsymbol{q}}$ of the electrical potential:

$$V_{\boldsymbol{q}} = \varphi_{\boldsymbol{q}} \frac{\epsilon_z q\kappa + \epsilon_\mathrm{b} q^2 \tanh(d\kappa)}{\epsilon_z q\kappa + (\epsilon_\mathrm{a}\epsilon_\mathrm{b} q^2 + \epsilon_z^2\kappa^2)\tanh(d\kappa)/(2\bar{\epsilon})} \,. \quad (1)$$

Here, $q = |\boldsymbol{q}|$, $\boldsymbol{q} = (q_x, q_y)$, $\kappa \equiv (\epsilon_x q_x^2/\epsilon_z + \epsilon_y q_y^2/\epsilon_z)^{1/2}$, and $\varphi_{\boldsymbol{q}} \equiv -2\pi e/(q\bar{\epsilon})$ with $\bar{\epsilon} = (\epsilon_\mathrm{a} + \epsilon_\mathrm{b})/2$. Eq. (1) is the most important result of this Section and reproduces all known elementary results. For example, in the limit $d \to 0$ Eq. (1) yields the potential of an electron in a graphene sheet embedded in two homogeneous and isotropic dielectrics, i.e. $V_{\boldsymbol{q}} \to \varphi_{\boldsymbol{q}}$. Similarly, for any finite d and for an isotropic medium with $\epsilon_x = \epsilon_y = \epsilon_z \equiv \epsilon_\mathrm{i}$, it is easy to check that Eq. (1) yields [2] $V_{\boldsymbol{q}} \to -4\pi e\cosh(\eta_\mathrm{a})\cosh(qd + \eta_\mathrm{b})/[q\epsilon_\mathrm{i}\sinh(qd + \eta_\mathrm{a} + \eta_\mathrm{b})]$ with $2\eta_{\mathrm{a,b}} = \ln[(\epsilon_\mathrm{i} + \epsilon_{\mathrm{a,b}})/(\epsilon_\mathrm{i} - \epsilon_{\mathrm{a,b}})]$. The ratio on the right-hand side of Eq. (1) can be interpreted as a form factor due to the presence of the anisotropic insulator slab, which dresses the "bare" 2D Coulomb potential $\varphi_{\boldsymbol{q}}$. For graphene on hBN, the relevant limit of Eq. (1) is that of a *uniaxial* dielectric medium with $\epsilon_y = \epsilon_x$. In this case Eq. (1) reduces to

$$V_{\boldsymbol{q},\omega} = \varphi_{\boldsymbol{q}} \frac{\sqrt{\epsilon_x\epsilon_z} + \epsilon_\mathrm{b}\tanh(qd\sqrt{\epsilon_x/\epsilon_z})}{\sqrt{\epsilon_x\epsilon_z} + (\epsilon_x\epsilon_z + \epsilon_\mathrm{b}\epsilon_\mathrm{a})\tanh(qd\sqrt{\epsilon_x/\epsilon_z})/(2\bar{\epsilon})} \,. \quad (2)$$

We have modified the notation of the Coulomb potential in Eq. (2) to explicitly indicate its dependence on frequency. Indeed, in the case of hBN, the components of the dielectric tensor have an important dependence on frequency in the mid infrared, which is usually parametrized in the following form [3]

$$\epsilon_\ell(\omega) = \epsilon_{\ell,\infty} + \frac{\epsilon_{\ell,0} - \epsilon_{\ell,\infty}}{1 - (\omega/\omega_\ell^\mathrm{T})^2 - i\gamma_\ell\hbar\omega/(\hbar\omega_\ell^\mathrm{T})^2} \,, \quad (3)$$

with $\ell = x$ or z. Here $\epsilon_{\ell,0}$ and $\epsilon_{\ell,\infty}$ are the static and high-frequency dielectric constants, respectively, while ω_ℓ^T is the transverse optical phonon frequency in the direction ℓ. The longitudinal optical phonon frequency ω_ℓ^L satisfies the Lyddane-Sachs-Teller relation $\omega_\ell^\mathrm{L} =$

	$\ell = x$	$\ell = z$
$\epsilon_{\ell,0}$	6.41	3.0
$\epsilon_{\ell,\infty}$	4.54	2.5
γ_ℓ (meV)	0.82	0.23
$\hbar\omega_\ell^\mathrm{T}$ (meV)	168.0	94.2
$\hbar\omega_\ell^\mathrm{L}$ (meV)	199.6	103.2

TABLE I. Microscopic parameters [4] entering Eq. (3).

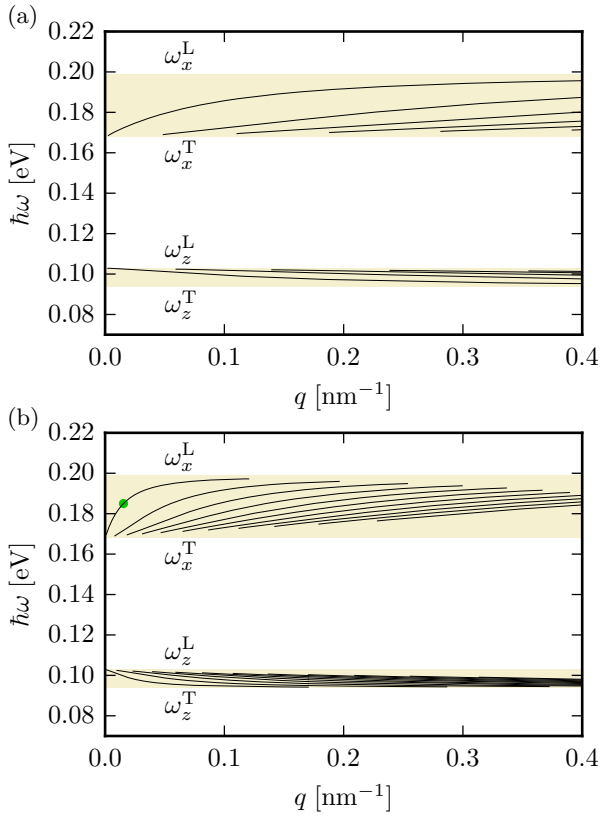

FIG. 1. (Color online) Dispersion of phonon-polaritons modes in a hBN slab. Poles of the dressed electrical potential $V_{\boldsymbol{q},\omega}$ in Eq. (2) are shown as functions of the wave vector $\boldsymbol{q}$. Here and in the following figures we use $\epsilon_{\rm a} = 1$ (vacuum) and $\epsilon_{\rm b} = 3.9$ (SiO_2). Panel (a) is for $d = 10$ nm, while panel (b) is for $d = 60$ nm. Shaded areas denote upper and lower reststrahlen bands. The green filled circle represents the point where the group velocity of the mode equals the graphene Fermi velocity $v_{\rm F}$. The 10 nm-thick slab does not support modes with group velocity equal to $v_{\rm F}$.

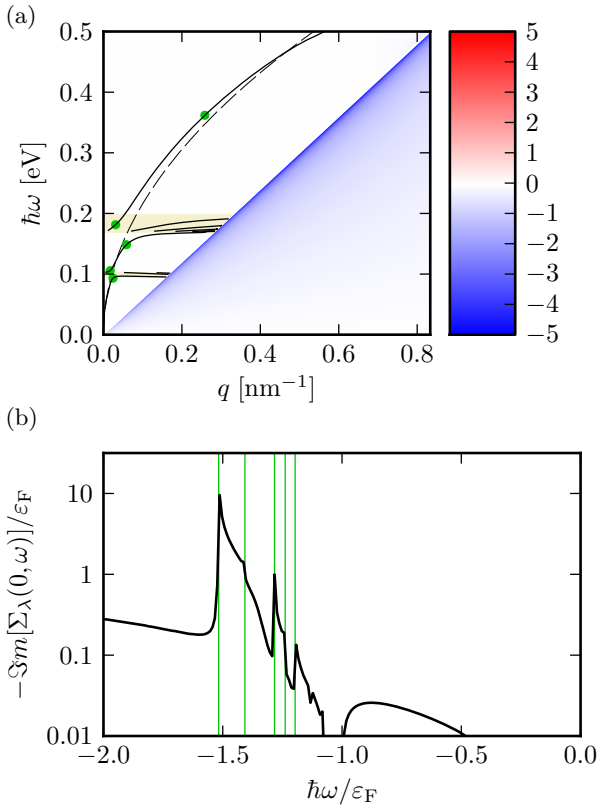

FIG. 2. (Color online) Panel (a) Plasmon-phonon polariton dispersion for a doped graphene sheet ($\varepsilon_{\rm F} = 400$ meV) on a 10 nm-thick hBN slab. The dashed line represents the dispersion relation of a Dirac plasmon in graphene in the absence of hBN phonons. Horizontal shaded areas and green filled circles have the same meaning as in Fig. 1. The density plot shows the imaginary part of the non-interacting polarization function in graphene and the corresponding colorbar is in units of the density of states at the Fermi energy. Panel (b) The quantity $-{\rm Im}[\Sigma_\lambda(\boldsymbol{k},\omega)]$ (in units of $\varepsilon_{\rm F}$ and evaluated at $\boldsymbol{k} = 0$) is shown as a function of the rescaled frequency $\hbar\omega/\varepsilon_{\rm F}$. Green vertical lines denote the values of $\hbar\omega/\varepsilon_{\rm F}$ at which a plasmon-phonon polariton peak is expected.

$\omega_\ell^{\rm T}\sqrt{\epsilon_{\ell,0}/\epsilon_{\ell,\infty}}$. The parameters in Eq. (3) are listed in Table I and have been taken from recent measurements [4] on high-quality *bulk* hBN [5]. A simple inspection of Eq. (3) in the limit $\gamma_\ell \to 0$ shows that, as we stated earlier, hBN is a hyperbolic material: in the lower (upper) reststrahlen band, which is defined by the inequality $\omega_z^{\rm T} < \omega < \omega_z^{\rm L}$ ($\omega_x^{\rm T} < \omega < \omega_x^{\rm L}$), the quantities $\epsilon_x\epsilon_z, \epsilon_x/\epsilon_z$ take negative values.

II. ANALYTICAL RESULTS ON THE DISPERSION PHONON-POLARITON MODES

In the limit $\gamma_\ell \to 0$ it is possible to obtain analytical expressions for the dispersion of phonon-polariton modes in a hBN slab (without a graphene sheet placed on top of it). We remind the reader that these modes are the solutions $\omega = \omega_{\boldsymbol{q}}$ of the equation $\sqrt{|\epsilon_x(\omega)\epsilon_z(\omega)|} + (2\bar{\epsilon})^{-1}[\epsilon_x(\omega)\epsilon_z(\omega) + \epsilon_{\rm b}\epsilon_{\rm a}]\tan[qd\sqrt{|\epsilon_x(\omega)/\epsilon_z(\omega)|}] = 0$.

Here, we report the results for the modes in the upper reststrahlen band. Similar expressions can be obtained for the lower reststrahlen band. For $qd \ll 1$, we find that one mode approaches the bottom of the reststrahlen band linearly

$$\omega_{\boldsymbol{q}} \to \omega_x^{\rm T}\left(1 + \frac{\epsilon_{x,0} - \epsilon_{x,\infty}}{4\bar{\epsilon}}\, qd + \dots\right) \qquad (4)$$

while the other modes decrease quadratically

$$\omega_{\boldsymbol{q}} \to \omega_x^{\rm T}\left[1 + \frac{1}{2}\frac{\epsilon_{x,0} - \epsilon_{x,\infty}}{\epsilon_z(\omega_x^{\rm T})}\left(\frac{qd}{n\pi}\right)^2 + \dots\right]. \qquad (5)$$

In the limit $qd \ll 1$ (with $n = 1, 2, \dots$), instead we find that all modes approach the upper end of the reststrahlen

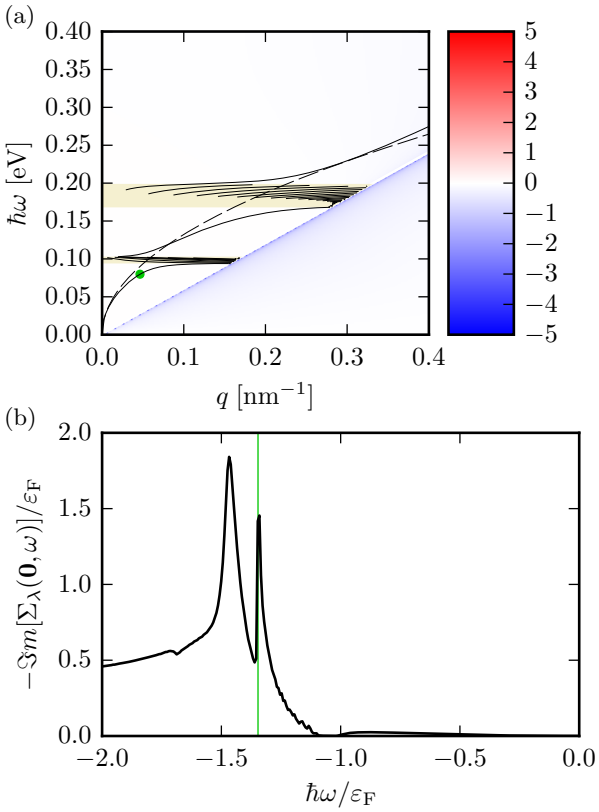

FIG. 3. (Color online) Same as Fig. 2 with parameters $\varepsilon_F = 150$ meV and $d = 60$ nm.

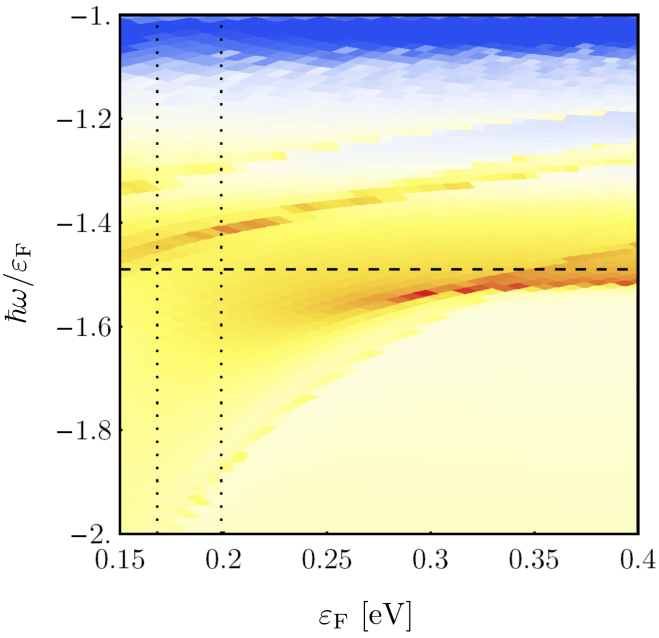

FIG. 4. (Color online) A 2D color plot of the quantity $-\mathrm{Im}[\Sigma_\lambda(\mathbf{0},\omega)]$ as a function of $\hbar\omega/\varepsilon_F$ and ε_F. Data in this plot refer to a hBN slab of thickness $d = 60$ nm. As usual, $\epsilon_a = 1$ and $\epsilon_b = 3.9$. The horizontal dashed line marks the expected position of a plasmon-phonon polariton peak in the absence of the hBN slab. The vertical dotted lines mark the extremes of the upper reststrahlen band.

band asymptotically

$$\omega_{\boldsymbol{q}} \to \omega_x^{\mathrm{L}} \left\{ 1 - \frac{1}{2}\epsilon_z(\omega_x^{\mathrm{L}}) \frac{\epsilon_{x,0} - \epsilon_{x,\infty}}{\epsilon_{x,\infty}\epsilon_{x,0}} \left(\frac{n\pi}{qd}\right)^2 + \dots \right\} . \tag{6}$$

III. ADDITIONAL NUMERICAL RESULTS

The following figures contain additional numerical results with respect to those included in the main text.

Figs. 2 and 3 show the plasmon-phonon polariton mode dispersion and the frequency dependence of the imaginary part of the quasiparticle self-energy. With respect to Figs. 2(a) and 2(b) in the main text, different values of hBN thickness and graphene Fermi energy are used in Fig. 2 and 3, respectively. In Fig. 2, we see that the dispersion of the plasmon-phonon polaritons changes with the hBN slab thicknes, and so does the wave vector where the group velocity of the modes equals the graphene Fermi velocity v_F. However, the connection between the modes slope and the peaks in the imaginary part of the quasiparticle self-energy persists. In Fig. 3, the lower chemical potential induces a less steep dispersion of the bare plasmon mode. This reflects in the fact that all the plasmon-phonon polariton modes are less steep and the number of points where the mode group velocity matches v_F is reduced from 7 [cfr. Figs. 2(a) of the main text] to 1. However, a large segment of the hybrid mode branch has *approximately* group velocity equal to v_F in the range $0.1\ \mathrm{nm}^{-1} \lesssim q \lesssim 0.3\ \mathrm{nm}^{-1}$ and $0.10\ \mathrm{eV} \lesssim \hbar\omega \lesssim 0.15\ \mathrm{eV}$. This results in an enhanced decay rate which appears as a broad peak of the imaginary part of the self-energy at $\hbar\omega/\varepsilon_F \simeq 1.5$.

The dependence of the decay rate (proportional to the imaginary part of the quasiparticle self-energy) on the Fermi energy is studied in detail in Fig. 4. We see that the decay rate depends smoothly on the Fermi energy and that there is no abrupt change in the imaginary part of the quasiparticle self-energy when the Fermi energy crosses the extremes of the upper reststrahlen band. Moreover, for large Fermi energies, the main peak in the imaginary part of the self-energy is due to a plasmon-polariton mode which exists also in the absence of the hBN. This mode corresponds to the higher-energy branch in Fig. 2(a) of the main text and in Fig. 2 and generates the spectral feature labeled by (2) in Fig. 1 of the main text. To see this, in Fig. 4 we plot (horizontal dashed line) the expected position of the plasmon-polariton peak in the absence of the hBN slab. This is easily found from the well-known dispersion of the graphene plasmon, which has group velocity equal to v_F at the wave

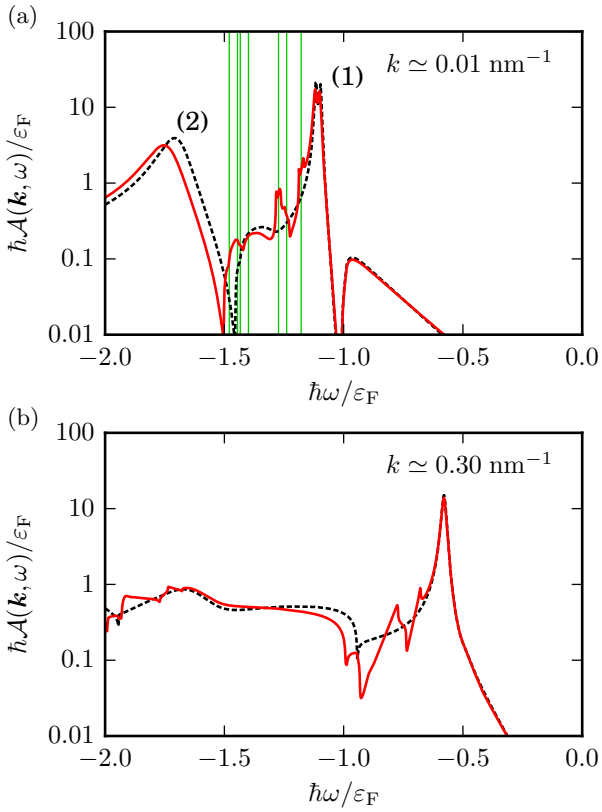

FIG. 5. (Color online) Frequency dependence of the quasiparticle spectral function $\mathcal{A}(\boldsymbol{k},\omega)$ for two values of k (indicated in the plots), corresponding to $k = 0.01$ and $0.5\ k_F$. The Fermi energy is $\varepsilon_F = 400$ meV. The red solid lines correspond to $d = 60$ nm, while the black dashed line correspond to $d = 0$. Panel (a) The vertical green lines correspond to the expected positions of the plasmon-phonon polariton peaks for $k \simeq 0$. The two spectral features labeled (1) and (2) correspond to those in Fig. 1 of the main text.

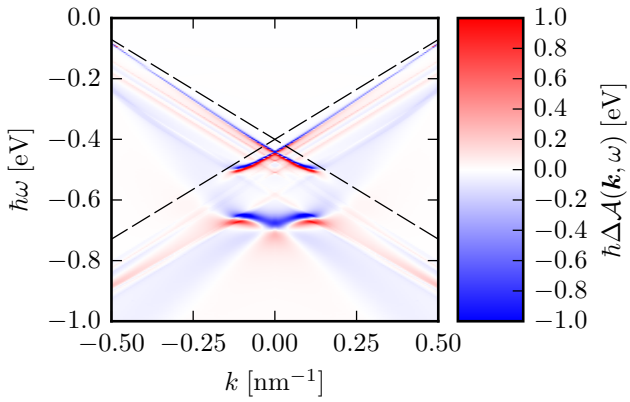

FIG. 6. (Color online) Difference between the spectral function $\mathcal{A}(\boldsymbol{k},\omega)$ for $d = 60$ nm and the spectral function calculated in the absence of the hBN slab, i.e. $d = 0$. The Fermi energy is $\varepsilon_F = 400$ meV. The dashed line indicates the Dirac cone. The redistribution of spectral weight due to the presence of the hBN slab is sizable.

vector $q^* = \varepsilon_F e^2/(\epsilon_a + \epsilon_b)$. Then, following the argument explained in the main text, we find that the peak in the imaginary part of the quasiparticle self-energy is expected at $\hbar\omega/\varepsilon_F = -e^2/(\hbar v_F \bar{\epsilon}) + \hbar v_F q_\parallel - 1 \simeq -1.5$, independent of other parameters. Satellite modes are clearly visible and drift to lower values of $\hbar\omega$ with decreasing Fermi energy. The main peak broadens as the upper reststrahlen band is approached, and eventually a satellite peak becomes more prominent and closer to the frequency $\hbar\omega/\varepsilon_F \simeq -1.5$ of the main plasmon-polariton mode.

Fig. 5 shows the frequency dependence of the quasiparticle spectral function at finite wave vector. Each panel shows the spectral function with (red solid line) and without (black dashed line) the hBN substrate. In Fig. 5(a), the quasiparticle peaks corresponding to conduction and valence band, labeled by (1), are very close in energy and barely resolved. The spectral feature at $\hbar\omega/\varepsilon_F \simeq -1.7$, labeled by (2), is due to the plasmon-polariton mode discussed above. The satellite peaks between (1) and (2) appear close to the frequencies where the peaks of the imaginary part of the quasiparticle self-energy are present. However, the expected position of the plasmon-polariton peak does not match its actual position (2). This effect is well-known and is a consequence of the attractive interaction between the emitted plasmon and the hole left behind by the photo-excited electron. [7] For the satellite peaks this effect is smaller as the frequency ω is increased. This can be understood from the plot of the imaginary part of the self-energy [Fig. 2(b) in the main text]: the plasmon-polariton peak has the largest decay rate, which obviously changes the position where the spectral function is maximal. The decay rate of the satellite peaks decreases as the frequency ω is increased. Inspecting Fig. 1 of the main text, we also note that $k \simeq 0$ or $k \lesssim k_F$ are the wave vector ranges where the satellite peaks could be more clearly seen, because at intermediate values of k they are obfuscated as they cross the broad spectral features (1) and (2). Fig. 5(b) shows that at intermediate values of k the peak corresponding to the conduction band is clearly seen, while the valence band peak is strongly damped and disappears in the continuum of excitations for $\hbar\omega \lesssim \varepsilon_F$.

Finally, Fig. 6 gives a more complete representation of the data shown in Fig. 5, by emphasizing the difference between the quasiparticle spectral function with and without the hBN substrate. The effect of the substrate is sizable, with variations in magnitude of the spectral function of order eV/$\hbar$. The spectral weight of both peaks (1) and (2) moves slightly to lower energies (i.e. the blue regions "move" to the red regions when d has a finite thickness). Moreover, the fine satellite bands are very clearly seen as an alternation of red and blue regions in this plot.

* levitov@mit.edu
† marco.polini@icloud.com

[1] L.D. Landau and E.M. Lifshitz, *Course of Theoretical Physics: Electrodynamics of Continuos Media* (Pergamon, New York, 1984).
[2] L.V. Keldysh, Pis'ma Zh. Eksp. Teor. Fiz. **29**, 716 (1979).
[3] R. Geick, C. H. Perry, and G. Rupprecht, Phys. Rev. **146**, 543 (1966).
[4] J.D. Caldwell, A. Kretinin, Y. Chen, V. Giannini, M.M. Fogler, Y. Francescato, C.T. Ellis, J.G. Tischler, C.R. Woods, A.J. Giles, M. Hong, K. Watanabe, T. Taniguchi, S.A. Maier, and K.S. Novoselov, Nature Commun. **5**, 5221 (2014).
[5] There is strong experimental evidence [6] that, due to fabrication, phonon losses in *thin* hBN tend to be larger than in bulk hBN. Rigorously speaking, the values of the parameters γ_ℓ given in Table I therefore provide only a lower bound on the phonon damping rates in thin hBN slabs.
[6] A. Woessner, M.B. Lundeberg, Y. Gao, A. Principi, P. Alonso-González, M. Carrega, K. Watanabe, T. Taniguchi, G. Vignale, M. Polini, J. Hone, R. Hillenbrand, and F.H.L. Koppens, Nature Mater. **14**, 421 (2015).
[7] A. Bostwick, F. Speck, T. Seyller, K. Horn, M. Polini, R. Asgari, A.H. MacDonald, and E. Rotenberg, Science **328**, 999 (2010).